Geochemistry Geophysics Geosystems G3
AN ELECTRONIC JOURNAL OF THE EARTH SCIENCES
Published by AGU and the Geochemical Society

Article
Volume 10, Number 11
19 November 2009
Q11011, doi:10.1029/2009GC002543
ISSN: 1525-2027

Evolving geometrical and material properties of fault zones in a damage rheology model

Vladimir Lyakhovsky
Geological Survey of Israel, Jerusalem 95501, Israel (vladi@geos.gsi.gov.il)

Yehuda Ben-Zion
Department of Earth Sciences, University of Southern California, Los Angeles, California 90089-0740, USA (benzion@usc.edu)

[1] We discuss numerical simulations of evolving fault zone structures in a 3-D lithospheric model with a seismogenic crust governed by a damage rheology that accounts for large strain associated with permanent brittle deformation. Results for the initial propagation of an existing narrow damage zone subjected to oblique loading exhibit strong asymmetry of the evolving damage with respect to the initial fault orientation and predict out-of-plane directions of the propagating damage zones. The orientations of the simulated damage zones agree with analytical expectations based on fracture mechanics for the directions of wing cracks generated at the tips of a crack under mixed mode loading. Lithosphere-scale numerical simulations for the long-term evolution of a large strike-slip fault zone produce initially a system of stepping en echelon segments associated with the asymmetric generation of new damage zones. The simulated fault zone segments evolve with continuing deformation to a throughgoing localized structure. Large-scale perturbation in the geometry of the Moho interface together with the regional heat regime can reduce considerably the degree of localization of the fault zone structure and the associated deformation fields.

Components: 7673 words, 8 figures, 1 table.

Keywords: damage rheology; brittle deformation; evolution of fault zones; numerical simulations.

Index Terms: 8020 Structural Geology: Mechanics, theory, and modeling; 8010 Structural Geology: Fractures and faults; 8004 Structural Geology: Dynamics and mechanics of faulting (8118).

Received 6 April 2009; **Revised** 8 September 2009; **Accepted** 5 October 2009; **Published** 19 November 2009.

Lyakhovsky, V., and Y. Ben-Zion (2009), Evolving geometrical and material properties of fault zones in a damage rheology model, *Geochem. Geophys. Geosyst.*, *10*, Q11011, doi:10.1029/2009GC002543.

1. Introduction

[2] Understanding the organization of distributed cracks and flaws to fault zones with concentrated damage, and subsequent evolution of the geometrical and material properties of the fault zones, is important for many topics including structural geology, earthquake and fault mechanics, engineering applications and seismic hazard assessments. In the present work, we use a thermodynamically based nonlinear continuum damage model for irreversible brittle deformation and a regional lithospheric framework [*Lyakhovsky and Ben-Zion*, 2008, and references therein] to study the spatio-temporal evolution of large strike-slip fault zones in several representative environments.

[3] It is well established from field studies [e.g., *Segall and Pollard*, 1983; *Willemse et al.*, 1997] and laboratory observations [e.g., *Broberg*, 1987; *Cox and Scholz*, 1988; *Lockner et al.*, 1991; *Ramsey and Chester*, 2004] that faults do not propagate into intact crystalline rock in their own planes as shear fractures. Instead, the growth process is associated with the interaction and coalescence of randomly oriented mode I microcracks in a process zone ahead of the propagating fault [*Reches and Lockner*, 1994; *Lyakhovsky*, 2001]. Recent laboratory studies of acoustic emission [*Stanchits et al.*, 2006] demonstrate clearly that tensile crack opening dominates during the early phases of loading, nucleation and fracture propagation in crystalline rocks. A wide variety of multidisciplinary observations summarized by *Ben-Zion and Sammis* [2003] indicate that newly created fault zones are characterized by highly irregular geometrical structures, and that continuing deformation leads to evolution from a disordered network of linked fault segments to simpler dominant localized fault zones [e.g., *Tchalenko*, 1970; *Wesnousky*, 1988; *Stirling et al.*, 1996; *Marco*, 2007].

[4] In section 4 we perform quantitative analyses of the evolution of large crustal fault zones using a 3-D lithospheric model consisting of a seismogenic crust governed by damage rheology over a viscoelastic substrate [*Ben-Zion and Lyakhovsky*, 2006; *Lyakhovsky and Ben-Zion*, 2008]. We first show that the initial trajectories of a preexisting narrow damage zone subjected to oblique loading agree well with the analytical solution of *Erdogan and Sih* [1963] for the propagation path of a crack under mixed loading conditions. This series of simulations connects classical fracture mechanics results with the employed continuum damage rheology. We demonstrate that the early evolution of a narrow damage zone mimics the growth of a single crack based on linear fracture mechanics. An advantage of the damage mechanics is that the modeling of the evolving damage zones may be extended far beyond the initial stage and implemented in a heterogeneous solid with multiple (rather than one dominant) failure zones. This is demonstrated by simulations of the nucleation and development of strike-slip fault zones in several realizations of a 3-D layered lithospheric model with various preexisting geometrical structures and heat regimes. The structural development in a basic model with planar horizontal boundaries between the layers is characterized by progressive evolution of the brittly deforming regions toward increasing localization and geometrical simplicity. A model realization with an assumed upward bulge in the topography of the Moho boundary produces persisting complexities of fault zone structures and related deformation fields.

2. Structural Evolution of Fracture Zone

[5] Mode I fractures have been studied extensively using linear elastic fracture mechanics (LEFM), and several criteria were introduced for the propagation of a predominantly mode I fracture under mixed mode loading conditions [*Erdogan and Sih*, 1963; *Cotterell and Rice*, 1980; *Cooke and Pollard*, 1996]. Attempts to produce a pure mode II shear fracture propagation in laboratory samples of low-porosity crystalline rocks, without a preexisting throughgoing failure zone, usually fail because opening fractures dominate the process. The available laboratory and theoretical results indicate that even a minor component of oblique loading may cause a deviation from the in-plane propagation of mode II fracture and blunt the crack front [*Erdogan and Sih*, 1963; *Cotterell and Rice*, 1980; *Cooke and Pollard*, 1996].

[6] A common form of brittle blunting consists of wing cracks that are produced off the continuation of the crack in a near-tip tensile region. There are different theoretical criteria for the propagation direction of wing cracks under mixed mode loading, which can hardly be distinguished experimentally [e.g., *Cooke and Pollard*, 1996]. The maximum tangential stress criterion of *Erdogan and Sih* [1963] implies that a crack loaded obliquely will grow radially from the crack tip in the direction along which the tangential stress, $\sigma_{\theta\theta}$, is maximum and the shear stress, $\sigma_{r\theta}$, is zero. Using polar coordinates r and θ centered at the fracture tip, the near-tip stresses are approximated by [*Sih et al.*, 1962]:

$$\begin{aligned}\sigma_{\theta\theta} &= \frac{1}{\sqrt{2r}}\mathrm{Cos}\left(\frac{\theta}{2}\right)\cdot\left[K_1\mathrm{Cos}^2\left(\frac{\theta}{2}\right)-\frac{3}{2}K_2\mathrm{Sin}(\theta)\right]\\ \sigma_{r\theta} &= \frac{1}{\sqrt{2r}}\mathrm{Cos}\left(\frac{\theta}{2}\right)\cdot\left[K_1\mathrm{Sin}(\theta)+K_2(3\mathrm{Cos}(\theta)-1)\right]\end{aligned} \quad (1)$$

For the case shown in Figure 1, where a preexisting crack with length $2a$ is loaded in tension by a force acting in the direction having an angle β to the

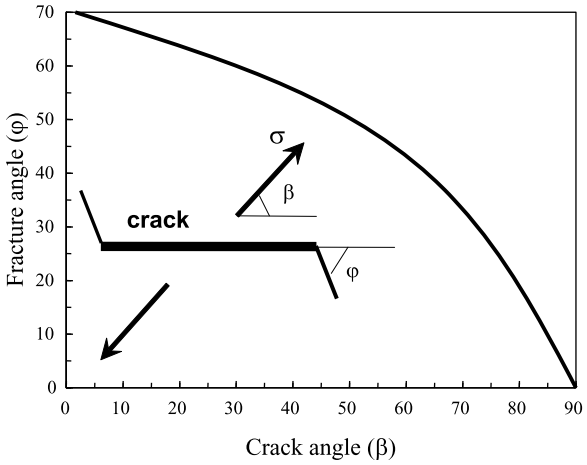

Figure 1. Expected analytical relation (equation (3)) between the load angle β from an existing crack and the fracture angle φ.

crack plane, the stress intensity factors K_1 and K_2 are given by [*Sih et al.*, 1962]:

$$K_1 = \sigma\sqrt{a}\cdot \mathrm{Sin}^2(\beta)$$
$$K_2 = \sigma\sqrt{a}\cdot \mathrm{Sin}(\beta)\cdot \mathrm{Cos}(\beta) \quad (2)$$

Using the stress intensity factors (2), the maximum tangential stress criterion of *Erdogan and Sih* [1963] predicts a fracture angle φ (Figure 1), which varies between 0° and 71° as a function of the crack angle

$$\mathrm{Sin}(\varphi) + (3\cdot \mathrm{Cos}(\varphi) - 1)\cdot \mathrm{Cot}(\beta) = 0. \quad (3)$$

The forgoing theoretical analysis of a kink angle based on LEFM predicts infinite stress at the crack tip [*Irwin*, 1957; *Rice*, 1968]. In spite of this unphysical singularity in the K dominant zone, the LEFM approach provides useful explanations for certain aspects of the observed deformation around dikes and faults [e.g., *Pollard and Segall*, 1987; *Willemse and Pollard*, 1998]. *Olson and Pollard* [1989] implemented the maximum tangential stress criterion into a boundary element numerical model and related the simulated curvature of joint traces to the magnitude of the remote stress. *Thomas and Pollard* [1993] compared the numerical predictions of *Olson and Pollard* [1989] to laboratory measured fracture paths and concluded that this approach is successful in predicting experimentally observed fracture paths.

[7] Real materials cannot sustain the large stresses in the K dominant zone and deform inelastically in a process zone that eliminates the stress singularity of LEFM. The process zone is often treated with models that include a cohesive zone near the crack tip within the plane of the crack [*Dugdale*, 1960; *Barenblatt*, 1962; *Ida*, 1972; *Palmer and Rice*, 1973; *Willemse and Pollard*, 1998]. As mentioned above, however, propagating cracks and faults are associated with evolving out-of-plane process zones and geometrical complexities. The damage zones generated near the crack tip modify the elastic moduli near those regions and affect the subsequent structural evolution [e.g., *Huang et al.*, 1991; *Chai*, 1993; *Zietlow and Labuz*, 1998].

[8] *Lyakhovsky* [2001] used the damage rheology model outlined in section 3 to simulate out-of-plane process zone and analyze aspects of the geometry and rate of a slowly growing crack. The simulated growth rate of straight mode I cracks were shown to fit well the experimentally observed power law relation, with a subcritical crack index depending on the ratio between the driving force and confining pressure. The geometry of the simulated process zone around the growing crack has a self-similar shape as predicted by the universal scaling of LEFM. In section 4.1 we analyze fault propagation under mixed mode I and mode II loading and demonstrate that the directions of newly created damage zones fit well the theoretical prediction of *Erdogan and Sih* [1963] on wing cracks and related laboratory experiments.

3. A Viscoelastic Damage Rheology Model

[9] Following earlier works, *Lyakhovsky and Myasnikov* [1985] and *Lyakhovsky et al.* [1997a, 1997b] developed a thermodynamically based nonlinear continuum damage rheology model for evolving elastic properties of rocks sustaining irreversible brittle deformation. The model generalizes the strain energy function of a solid to account for first-order macroscopic effects of existing cracks (damage), and makes the elastic moduli functions of an evolving damage state variable representing the local crack density. The developments are done within a framework of continuum mechanics and irreversible thermodynamics [e.g., *Onsager*, 1931; *Prigogine*, 1955; *Malvern*, 1969; *Kachanov*, 1986]. The results are applicable to volumes with a sufficiently large number of cracks that allow quantitative description through properties of the crack distribution rather than those of the individual cracks. The damage model accounts for three general aspects of brittle rock deformation: (1) mechanical response of a solid with an existing crack density, (2) kinetic changes associated with

the evolution of the crack density, and (3) dynamic aspect associated with macroscopic brittle instability. Detailed reviews and recent developments of the model in relation to phenomenology of earthquakes and faults are given by *Lyakhovsky and Ben-Zion* [2008] and *Ben-Zion* [2008]. Below we summarize the main ingredients of the model that are relevant for the present work.

3.1. Mechanical Response

[10] The mechanical effects of existing damage are modeled by generalizing the elastic strain energy function of a deforming solid to the form

$$U = \frac{1}{\rho}\left(\frac{\lambda}{2}I_1^2 + \mu I_2 - \gamma I_1\sqrt{I_2}\right), \tag{4}$$

where ρ is the mass density, $I_1 = \varepsilon_{kk}$ and $I_2 = \varepsilon_{ij}\varepsilon_{ij}$ are the first and second invariants of the elastic strain tensor ε_{ij}, λ and μ are the Lamé parameters of linear Hookean elasticity, and γ is a third modulus for a damaged solid. The first two terms of (4) give the classical strain potential of linear elasticity [*Malvern*, 1969]. The third term may be derived following the effective medium theory of *Budiansky and O'Connell* [1976], modified for effects of crack opening and closure in response to local tension or compression in the direction normal to the crack surface [*Lyakhovsky et al.*, 1997b]. The third term may be also obtained by expanding the strain energy potential as a general second-order function of the strain invariants and eliminating nonphysical terms of the expansion [*Ben-Zion and Lyakhovsky*, 2006].

[11] The nonlinear stress-strain relations derived from the potential (4) is consistent with detailed laboratory observations. These include experimentally measured changes of the effective elastic moduli under reversal of the stress from compression to tension [*Lyakhovsky et al.*, 1997a, 1997b, and references therein], rock dilation due to deviatoric stresses [*Hamiel et al.*, 2005] and additional results of rock mechanics experiments [*Lyakhovsky et al.*, 1993; *Hamiel et al.*, 2004, 2006]. Recently, *Hamiel et al.* [2009] demonstrated that the model fits well stress- and damage-induced seismic wave anisotropy observed during cycling load of Aue granite samples. The same formulation also explains observed changes in resonance curves of damaged materials under both low and high strain levels [*Lyakhovsky et al.*, 2009].

3.2. Damage Evolution

[12] The basic assumption leading to the equation for damage evolution is that in addition to the standard thermodynamic variables (strain tensor and temperature), the internal energy of a continuum solid, U, is a function of an independent scalar damage state variable, α, representing the local crack density. The elastic moduli are then functions of the damage state variable that evolves in the range $0 \le \alpha \le 1$. Using the balance equations of energy and entropy [*Lyakhovsky et al.*, 1997a], the damage-related entropy production density is represented as a product of a thermodynamic flux ($d\alpha/dt$) and a thermodynamic force ($\partial U/\partial\alpha$). Adopting the Onsager principle [*Onsager*, 1931] of linear relations between thermodynamic forces and fluxes, the equation of damage evolution has the form [*Lyakhovsky et al.*, 1997a]

$$\frac{d\alpha}{dt} = -C\frac{\partial U}{\partial \alpha}, \tag{5a}$$

where C is a positive function of state variables that ensures nonnegative local entropy production. Using the potential (4) in equation (5a), assuming for simplicity that the moduli $\mu(\alpha)$ and $\gamma(\alpha)$ are linear functions of α and that λ is constant, and keeping the leading term gives [*Lyakhovsky et al.*, 1997a]:

$$\frac{d\alpha}{dt} = \begin{cases} C_d I_2(\xi - \xi_0), & for \quad \xi \ge \xi_0 \\ C_1 \cdot \exp\left(\dfrac{\alpha}{C_2}\right) I_2(\xi - \xi_0), & for \quad \xi < \xi_0 \end{cases}. \tag{5b}$$

where $\xi = I_1/\sqrt{I_2}$ is referred to as the strain invariants ratio. The coefficient C_d gives the rate of positive damage evolution (material degradation) for $\xi > \xi_0$ and is constrained by laboratory fracturing experiments [*Lyakhovsky et al.*, 1997a; *Hamiel et al.*, 2004, 2009]. The rate of damage recovery (material healing) for state of strain $\xi < \xi_0$ is assumed in (5b) to depend exponentially on α. This produces logarithmic healing with time in agreement with the behavior observed in laboratory experiments [e.g., *Dieterich and Kilgore*, 1996; *Scholz*, 2002; *Johnson and Jia*, 2005] with rocks and other materials. *Lyakhovsky et al.* [2005] showed that the above damage model reproduces the main phenomenological features of rate- and state-dependent friction, and constrained the healing parameters C_1, C_2 by comparing model calculations with laboratory frictional results. The value $\xi = \xi_0$ controlling the transition from healing to damage accumulation is directly related to the

internal friction of intact rock [*Lyakhovsky et al.*, 1997a].

[13] Following the onset of positive damage evolution above the elastic limit at $\xi = \xi_0$, and before the final macroscopic failure, the model incorporates a gradual accumulation of inelastic strain, ε^i_{ij}. Comparisons between theoretical predictions, observed deformation and acoustic emission from laboratory experiments in granites and sandstones, led *Hamiel et al.* [2004] to suggest that the accumulation rate of the damage-related irreversible deformation is proportional to the rate of damage increase:

$$\frac{d\varepsilon^i_{ij}}{dt} = \begin{cases} C_v \dfrac{d\alpha}{dt}\tau_{ij} & \dfrac{d\alpha}{dt} > 0 \\ 0 & \dfrac{d\alpha}{dt} \le 0, \end{cases} \tag{6}$$

where C_v is a material constant and $\tau_{ij} = \sigma_{ij} - \sigma_{kk}\delta_{ij}/3$ is the deviatoric stress tensor. The damage-related compliance or inverse of viscosity ($C_v\, d\alpha/dt$) relates the deviatoric stress to the rate of irreversible strain accumulation. As in Maxwell viscoelasticity, the total strain tensor, $\varepsilon^t_{ij} = \varepsilon_{ij} + \varepsilon^i_{ij}$, is a sum of the elastic strain tensor and the inelastic component of deformation. This implies that the amount of irreversible strain that accumulates before the final macroscopic failure is proportional to the overall damage increase in the rock volume. Comparisons between model predictions and laboratory observations [*Hamiel et al.*, 2004, 2006, 2009] support the forgoing assumption and constrain the value of C_v. *Ben-Zion and Lyakhovsky* [2006] connected the rate of the gradual irreversible strain accumulation associated with equation (6) with partitioning between seismic and aseismic deformation in the seismogenic zone, and demonstrated that it is the major factor controlling properties of aftershock sequences.

3.3. Dynamical Aspect

[14] As the damage variable α increases, the modulus γ increases from 0 for a damage-free Hookean solid ($\alpha = 0$) to a maximum value γ_m, defined by normalization of the damage variable [*Lyakhovsky and Ben-Zion*, 2008]. The damage increase also leads to decreasing shear modulus, increasing Poisson ratio, and amplification of the nonlinearity of the effective rock elasticity. The process of damage increase becomes unstable with the loss of convexity of the potential (4), leading to macroscopic brittle instability at a critical level of damage [*Lyakhovsky et al.*, 1997a; *Lyakhovsky and Ben-Zion*, 2008]. The dynamic stress drop during the brittle instability produces a rapid release of the elastic energy and accumulation of a permanent plastic strain. The main physical assumptions of the mathematical procedure used by *Lyakhovsky and Ben-Zion* [2008] are that following the onset of brittle instability (loss of convexity), the damage level of the unstable volume increases rapidly to its maximal value ($\alpha = 1$) and the failing material undergoes frictional sliding. The slip associated with the macroscopic brittle failure is arrested and postfailure material healing starts when the strain invariant ratio is reduced to a fixed dynamic value ξ_d ($-\sqrt{3} \le \xi_d \le \xi_0$) corresponding to a residual dynamic friction level. The condition $\xi = \xi_d$ rewritten in terms of stresses (conjugate variables) is equivalent to Drucker-Prager plasticity with yielding parameters that are connected to dynamic friction of planar faults [see *Lyakhovsky and Ben-Zion*, 2008, equation 11 and Figure 3]. Simulations with the discussed model produce stress drops and scaling relations between rupture areas and seismic potency values that are consistent [*Lyakhovsky and Ben-Zion*, 2008] with classical theoretical results and observations summarized by *Kanamori and Anderson* [1975].

4. Structural Evolution of a Newly Created Damage Zone

4.1. Propagation Path Under Oblique Loading

[15] To test further model calculations against analytical results of LEFM, we study the propagation path of a preexisting narrow (one element thick) damage zone subjected to an oblique tension (Figure 1). Since the focus here is on overall changes of the geometry associated with brittle failure, we use a simplified version of the model without the gradual preinstability accumulation of inelastic strain associated with equation (6). The simulations employ the Fast Lagrangian Analysis of Continua (FLAC) algorithm [e.g., *Cundall and Board*, 1988; *Poliakov et al.*, 1993; *Ilchev and Lyakhovsky*, 2001] and each simulation ends after the propagation and arrest of the first macroscopic brittle failure. The geometry of the zone with elements where the damage achieved its critical value during the first macroscopic brittle event is compared to the predicted propagation direction of cracks under mixed mode loading [*Erdogan and Sih*, 1963].

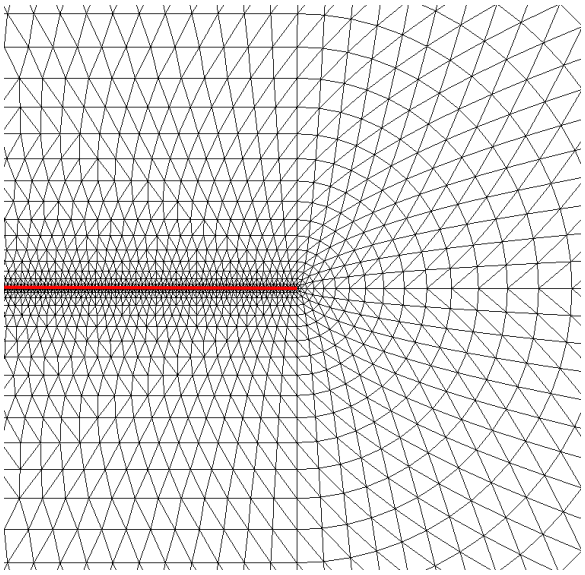

Figure 2. Mesh geometry around the tip of a preexisting narrow damage zone colored in red. The mesh consists of triangle elements with gradually increasing size away from the crack tip. The width of the damage zone (smallest element size) is one thousandth of the damage zone length.

[16] The simulations were done using the modified 3-D version of the code [*Ilchev and Lyakhovsky*, 2001] to meet 2-D plain stress conditions. Instead of 3-D tetrahedral elements, the reduced version uses triangle elements of variable sizes. The numerical solution based on the FLAC algorithm (as well as other numerical schemes) is sensitive to the size and orientation of the grid elements. To minimize this dependency the original FLAC-based 2-D code, *Poliakov et al.* [1993] used a double overlap of the triangle elements. The initial mesh of the model was made of quadrilaterals subdivided into two pairs of constant strain triangular elements. This allowed a reduction of the grid dependency at the expense of grid flexibility and computation time. The current version of the code drops the double overlapping and allows construction of a flexible triangular mesh with a wide range of element sizes. *Maimon et al.* [2005] showed that a good agreement between calculated stresses in a damage free (α = 0) material around a narrow damage zone (α = 1) and analytical solution for stress distribution around a single crack in linear elastic body is achieved when the element size (width of the damage zone) is reduced to one thousandth of the damage zone length.

[17] Both linear elasticity and the employed damage rheology are scale-independent, and the only length scales in related model calculations are associated with preexisting geometrical features such as the length of a preexisting crack or damage zone. The solutions using these frameworks are therefore self-similar, and depend on the distance from the crack (damage zone) tip scaled to the crack (damage zone) size. To minimize the dependency of the numerical solution on the orientation of the grid elements, the tip of the preexisting damage zone is surrounded by a fine mesh with element sizes that gradually increase up to hundred times away from the initial damage zone. Figure 2 displays a section of the mesh around the tip of the damage zone. Figure 3 shows the geometry of newly created damage zones, colored with blue, around the preexisting narrow damage zone (thick black line) under different loading conditions. The dotted green lines represent the predicted orientation of crack propagation based on equation (3). The orientations of the newly created high-damage zones, shown with red color in Figure 3, fit well the predicted paths of cracks under mixed mode I and mode II loading. Further propagation of the failing

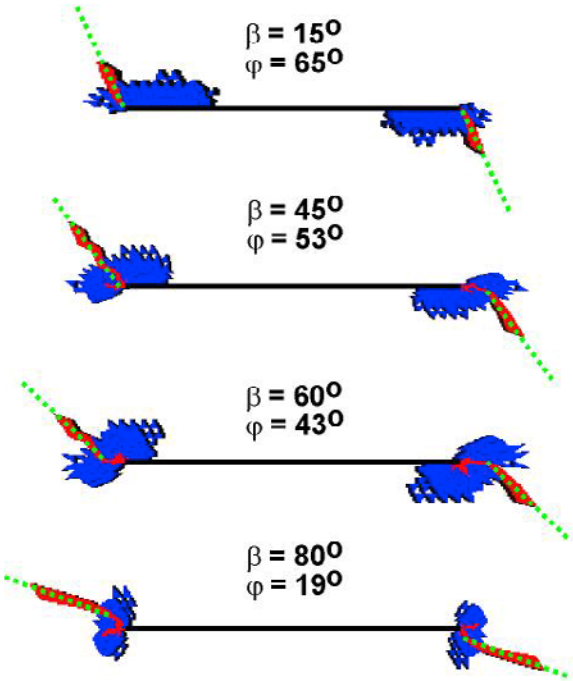

Figure 3. Geometry of simulated damage (blue) around a preexisting narrow fault zone (black) subjected to loading angles β = 15°, 45°, 60°, and 80°. The propagation paths of the generated highly damaged zones (red) follow the theoretically predicted directions (green dotted lines).

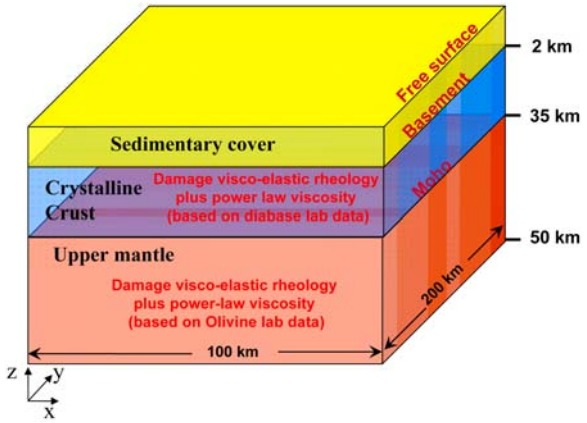

Figure 4. A schematic diagram of the 3-D lithospheric structure used in the numerical simulations.

elements is controlled not only by the loading conditions, but also by the interaction between the different damaged zones. This process is discussed in section 4.2 as part of regional-scale simulations. The results of Figure 3 confirm the ability of the damage rheology approach to reproduce branching paths of fault zones compatible with LEFM and laboratory observations under oblique loading.

4.2. Evolution of Fault Geometry With Cumulative Slip

[18] To simulate results relevant for earthquakes and crustal faults, we use the damage rheology in a 3-D regional model that includes three main units of the lithosphere (Figure 4). The upper layer represents a weak sedimentary cover, while the second and third layers represent the crystalline crust and upper mantle, respectively. *Ben-Zion and Lyakhovsky* [2006] provides a detailed description of the model setup.

[19] The total strain tensor ε_{ij}^t in each layer is written as the sum of three strain components associated with different deformation mechanisms

$$\varepsilon_{ij}^t = \varepsilon_{ij} + \varepsilon_{ij}^i + \varepsilon_{ij}^d, \tag{7}$$

where ε_{ij} is elastic strain related to the stress tensor through (4), ε_{ij}^i denotes the damage-related inelastic strain with accumulation rate calculated using (6), and ε_{ij}^d represents ductile strain. In the sedimentary layer the ductile strain is governed by Newtonian viscosity with $\eta = 10^{22}$ Pa·s, while in the lower crust and upper mantle it is governed by the power law relation [*Weertman*, 1978] between shear stress τ and strain rate $\dot{\varepsilon}$:

$$\dot{\varepsilon} = A\tau^n \exp\left(-\frac{Q + PV^*}{RT}\right). \tag{8}$$

The parameters A and n are empirical constants, Q is activation energy, V^* is activation volume, P is pressure, T is temperature, and R is the gas constant. For relatively low pressures corresponding to depths less than 100 km, the PV^* term in (8) is negligible.

[20] In the simulations below we use for the lower crust material constants $A = 6.31 \times 10^{-20}$ Pa^{-n}/s, $n = 3.05$, and $Q = 276$ kJ/mol appropriate for diabase rocks [*Carter and Tsenn*, 1987], and for the upper mantle constants $A = 1.9 \times 10^{-15}$ Pa^{-n}/s, $n = 3$, and $Q = 420$ kJ/mol appropriate for wet olivine [*Hirth and Kohlstedt*, 2003]. The simulations incorporate a depth-dependent temperature distribution, corresponding to a predefined surface heat flux. The temperature distribution significantly affects the ductile strain rate (8) and controls the depth of the seismogenic zone [*Ben-Zion and Lyakhovsky*, 2006]. The heat flux is therefore expected to have a significant impact on the style of strike-slip fault evolution. Two different cases are presented below, one for relatively cold lithosphere corresponding to 40 mW/m^2 surface heat flux, and another associated with a normal heat flux having 60 mW/m^2. We consider a model volume that is 100 km wide, 200 km long and 50 km deep (Figure 4). The volume is divided into tetrahedral elements of variable sizes that increase gradually from about 1 km in the seismogenic zone to about 5 km in the ductile region. This grid is sufficient to avoid significant computational errors related to the size of the numerical element and it allows the simulations to be done with a reasonable computation time. The size of the numerical element controls the smallest size of the simulated seismic events but has minor effects on the geometrical properties of the evolving fault zone.

[21] The boundary conditions, corresponding approximately to the Dead Sea transform region in Israel, consist of left-lateral plate motion with a rate of about 5 mm/year. The damage rheology model calculates the evolution of the elastic properties within the simulated volume, and leads to changes on the model boundaries that should be taken into account. In order to accommodate the external loading and internal changes, the forces acting on the boundaries should be updated during the simulation according to the mismatch (slip-deficit)

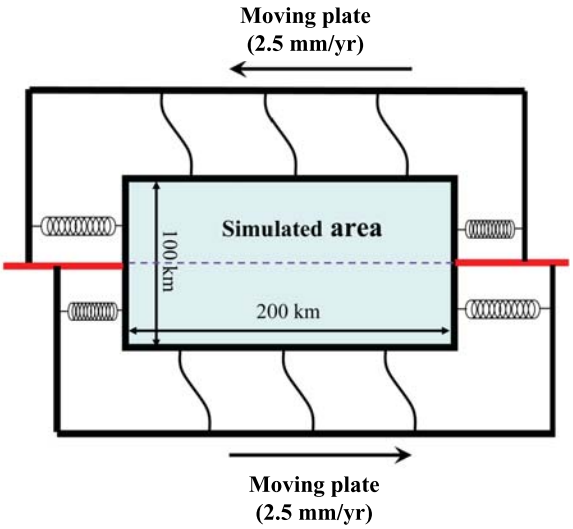

Figure 5. A schematic diagram illustrating the generalized boundary conditions corresponding to a constant plate motion far from the simulated model region. The red lines correspond to preexisting strike-slip faults outside the simulated volume.

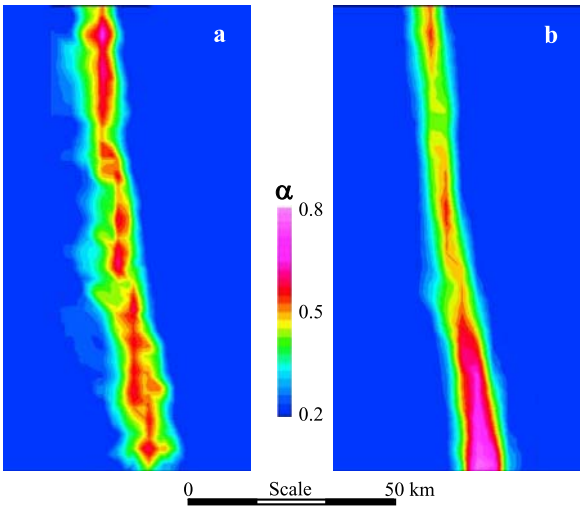

Figure 6. (a) Irregular damage pattern at an early stage of an evolving strike-slip fault zone. (b) Smooth damage pattern with a throughgoing fault zone after thousands of years of ongoing deformation. The temperature distribution corresponds to a surface heat flux of 40 mW/m^2.

between the far field plate motion and displacement of the boundary nodes. Following *Lyakhovsky and Ben-Zion* [2008], the boundary forces are equal to this mismatch multiplied by a stiffness of virtual springs connecting the boundary points to the far field plate motion (Figure 5). These boundary conditions are equivalent to a constant force in the limit of very large mismatch between the plate motion and the boundary nodes displacement. In the limit of very large spring stiffness, the applied boundary conditions become equivalent to constant velocity conditions. The potency-area scaling relations of simulated seismic events in models with spring stiffness values in the range St = 10^3–10^6 MPa/km are very similar for most events [*Lyakhovsky and Ben-Zion*, 2008]. However, very strong events may produce significant boundary displacement if the stiffness of the virtual springs is relatively low. In this case the seismic potency of the simulated event is overestimated. This effect disappears when the stiffness of the virtual springs is St = 10^5 MPa/km or higher. In the present study we use St = 10^5 MPa/km. The material parameters characterizing each model layer are listed in Table 1.

[22] Figure 6 illustrates the evolution of a large strike-slip fault zone with simulations employing the 3-D model. The temperature distribution corresponds to a surface heat flux of 40 mW/m^2. The applied boundary conditions include displacement discontinuities in the regions where the red lines, corresponding to preexisting strike-slip faults outside the simulated domain, cross the edges of the simulated volume. A fault zone nucleates near the left imposed discontinuity and propagates spontaneously inside the model volume. In agreement with the previous results, the simulated fault zone does not grow along a straight path. Instead, a system of left-stepping en echelon segments is first created (Figure 6a). At this stage a series of pull-

Table 1. Material Properties and Parameters of the Damage Rheology Model

Material Unit	Density (kg/m^3)	Elastic Moduli for Damage-Free Material (GPa)			Damage Rate Parameters (4)			Damage-Related Creep (Pa^{-1}), C_v
		λ_0	μ_0	ξ_0	C_d (s^{-1})	C_1 (s^{-1})	C_2	
Sedimentary layer	2400	14	18	−0.8	5	0.05	3×10^3	5.0×10^{-11}
Crust	2800	30	40	−0.8	5	0.05	3×10^3	1.2×10^{-11}
Upper mantle	3300	70	70	−0.8	5	0.05	3×10^3	3.0×10^{-11}

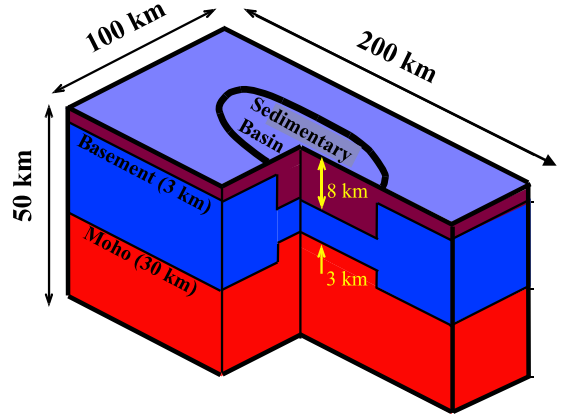

Figure 7. A diagram of a 3-D lithospheric structure with assumed uplift of the Moho interface and corresponding sedimentary basin.

apart basins are formed and accumulate some amount of opening. However, this geometrically complex structure is not stable for a long-term evolution of the fault zone. After thousands of years of deformation, and accumulation of tens of meters of slip across the fault zone, the irregularities become considerably smoother and the high-damage region becomes more localized (Figure 6b). The final configuration has a straight fault zone that cuts obliquely the whole seismogenic zone of the simulated volume. At larger depths, where ductile deformation dominates, the structure remains diffuse.

[23] In general, when the healing rate of damaged elements controlled by the values of C_1 and C_2 in equation (5b) is lower than the loading rate, the geometrical complexity of the fault zone evolves from initially disordered to smooth regular structure [*Ben-Zion et al.*, 1999; *Lyakhovsky et al.*, 2001]. The healing rate parameters may be constrained by combining available laboratory observations with geophysical and geodetic data [*Finzi et al.*, 2009]. The rate of the geometrical regularization process depends on the effective "brittleness" of the model region. The process of fault zone localization and reduction of geometrical complexities is more efficient in more "viscous" lithosphere, with higher background temperature associated with the higher surface heat flux, increased damage-related viscosity (high C_v values) and slower healing. High geometrical complexity is preserved for a longer time in more "brittle" lithosphere associated with the opposite set of conditions. The other parameters of the damage rheology model have minor effects on the evolving geometry of the fault zone. The value of ξ_0, which controls the onset of damage accumulation and is equivalent to the internal friction angle [*Lyakhovsky et al.*, 1997a], governs the stress level required for the nucleation of the fault zone. The rate of damage accumulation (C_d value) controls the time delay between the onset of damage accumulation and macroscopic brittle failure of the material element. This value is well constrained by the time span in rock mechanics experiments between the onset of acoustic emission and macroscopic sample failure [*Lyakhovsky et al.*, 1997a; *Hamiel et al.*, 2004, 2006, 2009]. In the regional-scale long-term simulations of the present paper, this short time delay has only minor effects on the evolution of the damage patterns.

[24] The generated structures and degree of strain localization can be affected significantly by the existence of large-scale geometrical and material heterogeneities. As an example, we consider a configuration with large preexisting deep sedimentary basin and corresponding Moho uplift (Figure 7). Such structures may be associated with preexisting magmatic intrusions in the upper mantle or sedimentary basins formed due to a previous local extension. The amount of uplift of the Moho interface isostatically compensates the presence of thick low-density sediments in the assumed basin. The Moho uplift, which replaces relatively ductile lower crust with mantle rocks, serves as a strong deep inclusion. Since the ductility of mantle rocks depends significantly on the temperature field, we present results for two model realizations (Figure 8). The first is associated with a relatively cold lithosphere having a temperature distribution corresponding to 40 mW/m^2 surface heat flux (Figures 8a–8c), and the second is associated with a normal lithosphere having 60 mW/m^2 (Figures 8d–8f).

[25] With accumulation of about 1 km displacement across the fault zone, the strain pattern in the seismogenic zone (10 km depth) is relatively simple in both cases (Figures 8a and 8d). Some local complexities associated with the large-scale perturbation of the Moho topography remain in the model corresponding to the colder lithosphere (Figures 8a–8c), whereas the model with normal heat flow environment exhibits high strain localization (Figures 8d–8f). At the base of the seismogenic zone (20 km depth) and around the Moho level (30 km depth), the differences between the strain patterns simulated by the two model realizations become more significant (Figures 8b and 8e). In the model with relatively cold lithosphere, the uplifted mantle block remains essentially undeformed and most of the deformation is localized

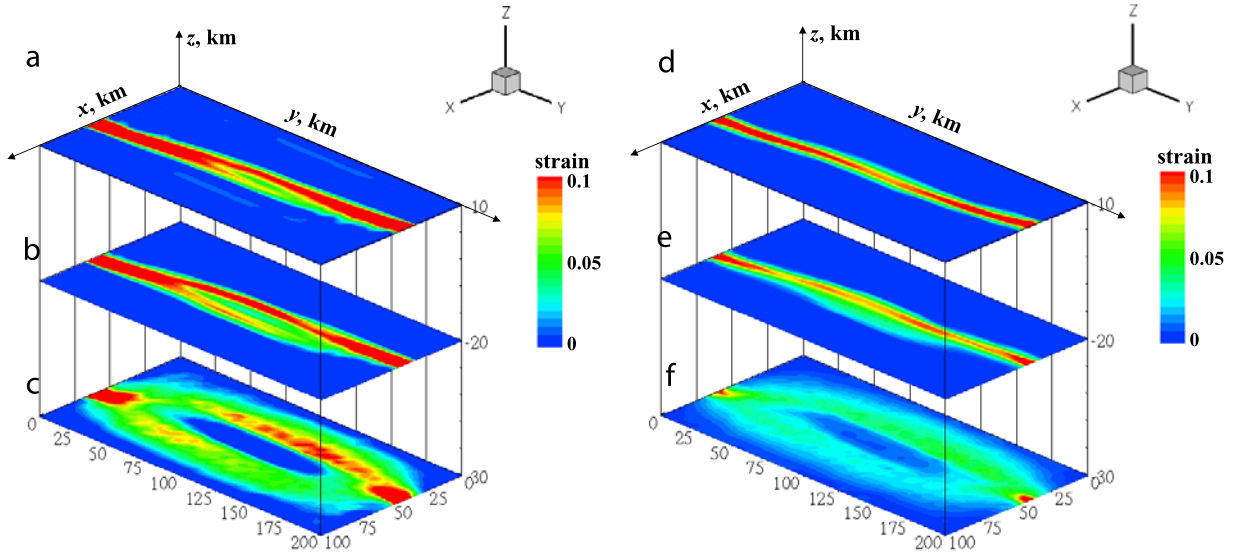

Figure 8. (a–c) Cumulative strain patterns at 10, 20, and 30 km depth after thousands of years of ongoing deformation in a model with temperature distribution corresponding to a surface heat flux of 40 mW/m^2. (d–f) Same as Figures 8a–8c but for temperature distribution corresponding to a surface heat flux of 60 mW/m^2.

at its periphery (Figure 8c). In the model with higher temperatures and heat flow, the uplifted mantle block sustains significant deformation and the resulting strain pattern is smoother also at the Moho base (Figure 8f). The results demonstrate that the deformation process in the upper mantle and resulting crustal fault zone structure can depend strongly on large-scale perturbations and the regional thermal regime.

5. Discussion

[26] The continuum damage mechanics employed in this study models the effects of distributed cracks in terms of a single scalar damage parameter α. Representative elementary volumes with a sufficiently large number of cracks corresponding to given values of α are assumed to be uniform and isotropic. However, the evolution and organization of the elementary damage zones, in response to external loadings and internal deformation, can produce macroscopic anisotropy and various patterns of large-scale fault zone structures [e.g., *Ben-Zion et al.*, 1999; *Lyakhovsky et al.*, 2001]. In addition, the asymmetric response of the damaged material to tensional and compressional loadings associated with the potential (4) leads to local seismic anisotropy in elementary damaged elements [*Hamiel et al.*, 2009]. The rate of evolution of material and geometrical properties of the generated fault zones is controlled by the form and coefficients of the kinetic equation (5b).

[27] *Lyakhovsky* [2001] demonstrated that the process zone created by distributed damage at the tip of a mode I crack eliminates the stress singularity of LEFM and provides a finite rate of quasi-static crack growth compatible with experimental observations. Here we provide an additional connection between the damage rheology and LEFM. As shown in Figure 3, the damage rheology model predicts a strong asymmetry of the process zone that is generated around the tip of a preexisting fault zone subjected to oblique loading. This asymmetry produces trajectories of the evolving newly created damage zones in out-of-plane directions that are in good agreement with the predicted directions of wing cracks under mixed mode I and mode II loading. The generated mixed I-II fracture modes govern the initial branching of the fault under oblique loading and contribute to the geometrical complexity of the fault zone at later evolutionary stages.

[28] Our 3-D simulations of a growing large strike-slip fault zone show evolution that is compatible with laboratory and field observations. A system of left-stepping en echelon segments is created at the initial stage of the fault evolution (Figure 6a). The initially complex system becomes progressively smoother with accumulation of displacements across the fault zone, and with tens of meters of total displacement the fault zone localizes into a narrow straight zone that cuts obliquely the model area (Figure 6b). In agreement with previous studies of coupled evolution of earthquakes and faults

in a vertically averaged rheologically layered lithosphere [*Ben-Zion et al.*, 1999; *Lyakhovsky et al.*, 2001], the evolution of the geometrical complexity of fault zones is controlled by the ratio between characteristic time scales of loading and healing. The time scale of loading is related primarily to the velocity of plate motion, while the healing time scale represents the complex thermo-chemical-mechanical processes of material recovery. Both time scales may vary between different regions and even within the same fault zone depending on the local tectonic rates, composition of the crustal rocks, temperature field, fluid content, etc. Fully 3-D simulations accounting for ductile strain components governed by the power law relations (8) enable us to compare the evolution of strike-slip fault zones in models with different temperature distributions. Elevated background temperature corresponding to a higher surface heat flux not only leads to a shallower seismogenic zone [*Ben-Zion and Lyakhovsky*, 2006], but also enhances significantly the localization and reduction of the geometrical complexity with the ongoing deformation.

[29] Large preexisting geometrical and material heterogeneities of the lithosphere can significantly affect the process of fault zone evolution. An examined configuration with preexisting deep sedimentary basin and corresponding Moho uplift (Figure 7) leads to long-living distributed deformation throughout the entire seismogenic zone in a model realization with a low heat flux of 40 mW/m^2 (Figures 8a–8c). The effects of the large-scale perturbation are reduced (e.g., Figures 8d–8f) in model realizations with lower effective viscosity associated with higher background temperature (heat flux 60 mW/m^2), increased damage-related viscosity and slower healing. A more detailed parameter space study of evolving large strike-slip fault zone structures and associated deformation fields is given by *Finzi et al.* [2009].

Acknowledgments

[30] We thank the editor Luc Lavier and two anonymous referees for constructive reviews. The studies were supported by the Israel Science Foundation (ISF 753/08) and the Southern California Earthquake Center (based on NSF Cooperative Agreement EAR-0106924 and USGS Cooperative Agreement 02HQAG0008).

References

Barenblatt, G. I. (1962), Mathematical theory of equilibrium cracks in brittle fracture, *Adv. Appl. Mech.*, *7*, 55–129, doi:10.1016/S0065-2156(08)70121-2.

Ben-Zion, Y. (2008), Collective behavior of earthquakes and faults: Continuum-discrete transitions, evolutionary changes, and corresponding dynamic regimes, *Rev. Geophys.*, *46*, RG4006, doi:10.1029/2008RG000260.

Ben-Zion, Y., and V. Lyakhovsky (2006), Analysis of aftershocks in a lithospheric model with seismogenic zone governed by damage rheology, *Geophys. J. Int.*, *165*, 197–210, doi:10.1111/j.1365-246X.2006.02878.x.

Ben-Zion, Y., and C. Sammis (2003), Characterization of fault zones, *Pure Appl. Geophys.*, *160*, 677–715, doi:10.1007/PL00012554.

Ben-Zion, Y., K. Dahmen, V. Lyakhovsky, D. Ertas, and A. Agnon (1999), Self-driven mode switching of earthquake activity on a fault system, *Earth Planet. Sci. Lett.*, *172*, 11–21, doi:10.1016/S0012-821X(99)00187-9.

Broberg, K. B. (1987), On crack path, *Eng. Fract. Mech.*, *28*, 663–679, doi:10.1016/0013-7944(87)90060-9.

Budiansky, B., and R. J. O'Connell (1976), Elastic moduli of a cracked solid, *Int. J. Solids Struct.*, *12*, 81–97, doi:10.1016/0020-7683(76)90044-5.

Carter, N. L., and M. C. Tsenn (1987), Flow properties of continental lithosphere, *Tectonophysics*, *136*, 27–63, doi:10.1016/0040-1951(87)90333-7.

Chai, H. (1993), Observation of deformation and damage at the tip of cracks in adhesive bonds loaded in shear and assessment of a criterion for fracture, *Int. J. Fract.*, *60*, 311–326.

Cooke, M. L., and D. D. Pollard (1996), Fracture propagation paths under mixed mode loading within rectangular blocks of polymethyl methacrylate, *J. Geophys. Res.*, *101*, 3387–3400, doi:10.1029/95JB02507.

Cotterell, B., and J. R. Rice (1980), Slightly curved or kinked cracks, *Int. J. Fract.*, *16*, 155–169, doi:10.1007/BF00012619.

Cox, S. J. D., and C. H. Scholz (1988), Rupture initiation in shear fracture of rocks: An experimental study, *J. Geophys. Res.*, *93*, 3307–3320, doi:10.1029/JB093iB04p03307.

Cundall, P. A., and M. Board (1988), A microcomputer program for modeling large-strain plasticity problems, in *Numerical Methods in Geomechanics: Proceedings of the 6th International Conference on Numerical Methods in Geomechanics, Innsbruck*, edited by C. Swoboda, pp. 2101–2108, A. A. Balkema, Rotterdam, Netherlands.

Dieterich, J. H., and B. D. Kilgore (1996), Imaging surface contacts; power law contact distributions and contact stresses in quarts, calcite, glass, and acrylic plastic, *Tectonophysics*, *256*, 219–239, doi:10.1016/0040-1951(95)00165-4.

Dugdale, D. S. (1960), Yielding of steel sheets containing slits, *J. Mech. Phys. Solids*, *8*, 100–104, doi:10.1016/0022-5096(60)90013-2.

Erdogan, F., and G. C. Sih (1963), On the crack extension in plates under plane loading and transverse shear, *J. Basic Eng.*, *85*, 519–527.

Finzi, Y., E. H. Hearn, Y. Ben-Zion, and V. Lyakhovsky (2009), Structural properties and deformation patterns of evolving strike-slip faults: Numerical simulations incorporating damage rheology, *Pure Appl. Geophys.*, *166*, 1537–1573, doi:10.1007/s00024-009-0522-1.

Hamiel, Y., Y. Liu, V. Lyakhovsky, Y. Ben-Zion, and D. Lockner (2004), A visco-elastic damage model with applications to stable and unstable fracturing, *Geophys. J. Int.*, *159*, 1–11, doi:10.1111/j.1365-246X.2004.02452.x.

Hamiel, Y., V. Lyakhovsky, and A. Agnon (2005), Rock dilation, nonlinear deformation, and pore pressure change under shear, *Earth Planet. Sci. Lett.*, *237*, 577–589, doi:10.1016/j.epsl.2005.06.028.

Hamiel, Y., O. Katz, V. Lyakhovsky, Z. Reches, and Y. Fialko (2006), Stable and unstable damage evolution in rocks with implications to fracturing of granite, *Geophys. J. Int.*, *167*, 1005–1016, doi:10.1111/j.1365-246X.2006.03126.x.

Hamiel, Y., V. Lyakhovsky, S. Stanchits, G. Dresen, and Y. Ben-Zion (2009), Brittle deformation and damage-induced seismic wave anisotropy in rocks, *Geophys. J. Int.*, *178*, 901–909, doi:10.1111/j.1365-246X.2009.04200.x.

Hirth, G., and D. L. Kohlstedt (2003), Rheology of the upper mantle and the mantle wedge: A view from the experimentalists, in *Inside the Subduction Factory*, *Geophys. Monogr. Ser.*, vol. 138, edited by J. Eiler, pp. 83–105, AGU, Washington, D. C.

Huang, W.-L., B. Kunin, and A. Chudnovsky (1991), Kinematics of damage zone accompanying curved crack, *Int. J. Fract.*, *50*, 143–152, doi:10.1007/BF00035209.

Ida, Y. (1972), Cohesive force across the tip of longitudinal shear crack and Griffith's specific surface energy, *J. Geophys. Res.*, *77*, 3796–3805, doi:10.1029/JB077i020p03796.

Ilchev, A., and V. Lyakhovsky (2001), Practical aspects of the hybridization of the boundary integral method with damage rheology modeling for the assimilation of seismic data, in *Dynamic Rock Mass Response to Mining, Rockbursts and Seismicity in Mines—RaSiM5*, edited by G. van Aswegen, R. J. Durrheim, and W. D. Ortlepp, pp. 421–426, S. Afr. Inst. of Min. and Metal., Johannesburg.

Irwin, G. R. (1957), Analyses of stresses and strains near the end of a crack traversing a plate, *J. Appl. Mech.*, *24*, 361–364.

Johnson, P. A., and X. Jia (2005), Non-linear dynamics, granular media and dynamic earthquake triggering, *Nature*, *437*, 871–874, doi:10.1038/nature04015.

Kachanov, L. M. (1986), *Introduction to Continuum Damage Mechanics*, 135 pp., Martinus Nijhoff, Dordrecht, Netherlands.

Kanamori, H., and D. L. Anderson (1975), Theoretical basis of some empirical relations in seismology, *Bull. Seismol. Soc. Am.*, *65*, 1073–1095.

Lockner, D. A., J. D. Byerlee, V. Kuksenko, A. Ponomarev, and A. Sidorin (1991), Quasi-static fault growth and shear fracture energy in granite, *Nature*, *350*, 39–42, doi:10.1038/350039a0.

Lyakhovsky, V. (2001), Scaling of fracture length and distributed damage, *Geophys. J. Int.*, *144*, 114–122, doi:10.1046/j.0956-540X.2000.01303.x.

Lyakhovsky, V., and Y. Ben-Zion (2008), Scaling relations of earthquakes and aseismic deformation in a damage rheology model, *Geophys. J. Int.*, *172*, 651–662, doi:10.1111/j.1365-246X.2007.03652.x.

Lyakhovsky, V., and V. P. Myasnikov (1985), On the behavior of visco-elastic cracked solid, *Izv. Acad. Sci. USSR Phys. Solid Earth, Engl. Transl.*, *4*, 28–35.

Lyakhovsky, V., Y. Podladchikov, and A. Poliakov (1993), Rheological model of a fractured solid, *Tectonophysics*, *226*, 187–198, doi:10.1016/0040-1951(93)90117-3.

Lyakhovsky, V., Y. Ben-Zion, and A. Agnon (1997a), Distributed damage, faulting, and friction, *J. Geophys. Res.*, *102*, 27,635–27,649, doi:10.1029/97JB01896.

Lyakhovsky, V., Z. Reches, R. Weinberger, and T. E. Scott (1997b), Non-linear elastic behavior of damaged rocks, *Geophys. J. Int.*, *130*, 157–166, doi:10.1111/j.1365-246X.1997.tb00995.x.

Lyakhovsky, V., Y. Ben-Zion, and A. Agnon (2001), Earthquake cycle, faults, and seismicity patterns in rheologically layered lithosphere, *J. Geophys. Res.*, *106*, 4103–4120, doi:10.1029/2000JB900218.

Lyakhovsky, V., Y. Ben-Zion, and A. Agnon (2005), A visco-elastic damage rheology and rate- and state-dependent friction, *Geophys. J. Int.*, *161*, 179–190, doi:10.1111/j.1365-246X.2005.02583.x.

Lyakhovsky, V., Y. Hamiel, P. Ampuero, and Y. Ben-Zion (2009), Non-linear damage rheology and wave resonance in rocks, *Geophys. J. Int.*, *178*, 910–920.

Maimon, O., V. Lyakhovsky, A. Agnon, and M. Abelson (2005), Stability of cavities and formation of sinkholes along the Dead Sea coast (in Hebrew with English abstract), *Isr. Geol. Surv. Rep. GSI/19/05*, 59 pp., Geol. Surv. Isr., Jerusalem.

Malvern, L. E. (1969), *Introduction to the Mechanics of a Continuum Medium*, 713 pp., Prentice-Hall, Upper Saddle River, N. J.

Marco, S. (2007), Temporal variation in the geometry of a strike-slip fault zone: Examples from the Dead Sea Transform, *Tectonophysics*, *445*, 186–199, doi:10.1016/j.tecto.2007.08.014.

Olson, J. E., and D. D. Pollard (1989), Inferring paleostresses from natural fracture patterns: A new method, *Geology*, *17*, 345–348, doi:10.1130/0091-7613(1989)017<0345:IPFNFP>2.3.CO;2.

Onsager, L. (1931), Reciprocal relations in irreversible processes, *Phys. Rev.*, *37*, 405–416, doi:10.1103/PhysRev.37.405.

Palmer, A. C., and J. R. Rice (1973), The growth of slip surfaces in the progressive failure of over-consolidated clay, *Proc. R. Soc. London, Ser. A*, *332*, 527–548.

Poliakov, A., P. A. Cundall, Y. Podladchikov, and V. Lyakhovsky (1993), An explicit inertial method for the simulation of viscoelastic flow: An evaluation of elastic effects on diapiric flow in two- and three-layers model, in *Proceedings of the NATO Advanced Study Institute on Dynamic Modeling and Flow in the Earth and Planets*, edited by K. E. Runcorn and D. Stone, pp. 175–195, Kluwer, Dordrecht, Netherlands.

Pollard, D. D., and P. Segall (1987), Theoretical displacements and stresses near fracture in rock: With applications to faults, joints, veins, dikes, and solution surfaces, in *Fracture Mechanics of Rocks*, edited by B. K. Atkinson, pp. 277–349, Academic, San Diego, Calif.

Prigogine, I. (1955), *Introduction to Thermodynamics of Irreversible Processes*, Thomas, Springfield, Ill.

Ramsey, J. M., and F. M. Chester (2004), Hybrid fracture and the transition from extension fracture to shear fracture, *Nature*, *428*, 63–66, doi:10.1038/nature02333.

Reches, Z., and D. A. Lockner (1994), Nucleation and growth of faults in brittle rocks, *J. Geophys. Res.*, *99*, 18,159–18,173, doi:10.1029/94JB00115.

Rice, J. R. (1968), Mathematical analysis in the mechanics of fracture, in *Fracture: An Advanced Treatise*, edited by H. Leibowitz, pp. 191–311, Academic, San Diego, Calif.

Scholz, C. H. (2002), *The Mechanics of Earthquakes and Faulting*, 2nd ed., 471 pp., Cambridge Univ. Press, New York.

Segall, P., and D. D. Pollard (1983), Nucleation and growth of strike slip faults in granite, *J. Geophys. Res.*, *88*, 555–568, doi:10.1029/JB088iB01p00555.

Sih, G. C., P. C. Paris, and F. Erdogan (1962), Crack tip stress intensity factors for plane extension and plate bending problems, *J. Appl. Mech.*, *84*, 306–312.

Stanchits, S., S. Vinciguerra, and G. Dresen (2006), Ultrasonic velocities, acoustic emission characteristics and crack damage of basalt and granite, *Pure Appl. Geophys.*, *163*, 975–994, doi:10.1007/s00024-006-0059-5.

Stirling, M. W., S. G. Wesnousky, and K. Shimazaki (1996), Fault trace complexity, cumulative slip, and the shape of the

magnitude-frequency distribution for strike-slip faults: A global survey, *Geophys. J. Int.*, *124*, 833–868, doi:10.1111/j.1365-246X.1996.tb05641.x.

Tchalenko, J. S. (1970), Similarities between shear zones of different magnitudes, *Geol. Soc. Am. Bull.*, *81*, 1625–1640, doi:10.1130/0016-7606(1970)81[1625:SBSZOD]2.0.CO;2.

Thomas, A. L., and D. D. Pollard (1993), The geometry of echelon fractures in rock: Implications from laboratory and numerical experiments, *J. Struct. Geol.*, *15*, 323–334, doi:10.1016/0191-8141(93)90129-X.

Weertman, J. (1978), Creep laws for the mantle of the Earth, *Philos. Trans. R. Soc. London, Ser. A*, *288*, 9–26, doi:10.1098/rsta.1978.0003.

Wesnousky, S. (1988), Seismological and structural evolution of strike-slip faults, *Nature*, *335*, 340–342, doi:10.1038/335340a0.

Willemse, E. J. M., and D. D. Pollard (1998), On the orientation and patterns of wing cracks and solution surfaces at the tip of a sliding flaw or fault, *J. Geophys. Res.*, *103*, 2427–2438, doi:10.1029/97JB01587.

Willemse, E. J. M., D. C. P. Peacock, and A. Aydin (1997), Nucleation and growth of strike-slip faults in limestones from Somerset, U. K., *J. Struct. Geol.*, *19*, 1461–1477, doi:10.1016/S0191-8141(97)00056-4.

Zietlow, W. K., and J. F. Labuz (1998), Measurements of the intrinsic process zone in rock using acoustic emission, *Int. J. Rock Mech. Min. Sci.*, *35*, 291–299, doi:10.1016/S0148-9062(97)00323-9.